International Journal of Naval Architecture and Ocean Engineering 11 (2019) 851–857

Contents lists available at ScienceDirect

International Journal of Naval Architecture and Ocean Engineering

journal homepage: http://www.journals.elsevier.com/international-journal-of-naval-architecture-and-ocean-engineering/

Robust sliding mode control for a USV water-jet system

HyunWoo Kim, Jangmyung Lee*

Pusan National University, South Korea

ARTICLE INFO

Article history:
Received 10 November 2018
Received in revised form
28 February 2019
Accepted 16 April 2019
Available online 26 April 2019

Keywords:
USV
Steering system
Sliding mode control
Disturbance
State observer

ABSTRACT

A new robust sliding mode control with disturbance and state observers has been proposed to control the nozzle angle of a water-jet system for a Unmanned Surface Vehicle (USV). As the water-jet system of a ship is subjected to direct disturbances owing to the exposure to the marine environment in water, it requires a robust control. A state observer and a disturbance observer are added to the water jet nozzle control system to achieve a robust control against disturbances. To verify the performance of the proposed algorithm, a test bed is constructed by a propulsion system used in the popular USV. This proposed algorithm has been evaluated by comparing to the existing algorithm through experiments. The results show that the performance of the proposed algorithm is better than that of the conventional PID or sliding mode controller when controlling the steering of the USV with disturbances.

1. Introduction

This study aims to propose a robust control of the nozzle angle of a water-jet against disturbances, which is the most critical factor for the steering control of an unmanned ship. Unmanned ships are maneuverable by nonhuman computers and many studies were actively carried out for safe navigation of ships (Huntsberger and Woodward, 2011; Bingham et al., 2010). Among these studies, path tracking and avoidance of obstacles were conducted as the most basic studies (Wu et al., 2009; Yu-minXu and Pang, 2006). The abovementioned studies were carried out under the Assumption that the steering apparatus of the ship could be effectively controlled to control the path of the ship (Son and Yoon, 2009). Especially, the accuracy of the steering is very important for a small USV that are running at a speed of 30 knots or more. If the accuracy of the ship steering during running is low, it will seriously affect the stability of the ship. However, although the steering system of a ship is subjected to direct disturbances owing to exposure to the marine environment in water and requires robust control, studies on this issue are scant (GONG et al., 2017).

The steering system of an unmanned ship is a typical nonlinear system such as a hydraulic system. Proportional–integral–derivative (PID) controllers have been utilized in most studies because they are convenient to use without modeling the control object (Yoo and Ryu, 2016). The PID controller does not reflect the nonlinearity of the system, and hence, it is difficult to control an Unmanned Surface Vehicle (USV) robustly and stably. In addition, disturbances occurring in the system cannot be coped with. In this study, the nonlinearity of the system is reflected by using a Sliding Mode Controller (SMC), which is a typical nonlinear controller, for robust and stable control of the nonlinear hydraulic system.

The SMC is very widely used because of its robustness to disturbance and parameter uncertainty (Utkin et al., 2009). SMC is a nonlinear control system with the dynamics of a nonlinear system by application of a discontinuous control signal that forces the system to slide onto a particular surface, called a sliding surface. The hydraulic actuator is defined by three state variables. The system consists of numerous variables, and the controller is required to be configured for higher-order SMC. In higher-order SMC, the state variable should be estimated in order to construct the SMC model. The state variable can be estimated effectively by using an observer (Iwan et al., 2017). A disturbance observer was added to the robust sliding mode to estimate the disturbances that occur during the operation of the ship. Therefore, the robust sliding mode including the state observer and disturbance observer can cope with the disturbance of the USV system. In order to verify the performance of the algorithm proposed in this paper, a test bed was constructed using the same specification system as the propulsion system used in the USV. We compared the performance of the proposed algorithm with that of the existing algorithm through

* Corresponding author.
E-mail address: jmlee@pusan.ac.kr (J. Lee).
Peer review under responsibility of Society of Naval Architects of Korea.

https://doi.org/10.1016/j.ijnaoe.2019.04.001

experiments using the test bed.

Therefore, in this study, the mathematical model of a hydraulic system is analyzed to design the control system in Section 2. In Section 3, an SMC and a disturbance and state observer are designed for application to a nonlinear hydraulic water-jet system. In order to verify the performance of the controller and observer developed in Section 4, we perform simulation before the actual application. In Section 5, the developed SMC and observer are applied to an actual test bed to confirm the effectiveness of the proposed algorithm through the real experiments. Finally, in Section 6, this paper is concluded with an emphasis on its contributions.

2. System modeling of the water-jet system

The major assumptions used in the modeling are as follows:

1) The values of parameters are assumed to vary within known boundaries of nominal values.
2) Frictional force between the cylinder wall and piston can be neglected.
3) Leakage flow of fluid in the cylinder and valve can be neglected.
4) Spool in the valve is critically lapped.

Fig. 1 illustrates the configuration of the hydraulic servo system for the water-jet (Merrit, 1967; Chen and Wu, 1992). In Fig. 1, the upper part shows the servo valve and the lower part shows the hydraulic piston. When the current is applied to the servo valve as the control input, the spool controlling the hydraulic pressure moves. The relation between the position of the spool (x_v) and the input current (i) can be defined as follows:

$$x_v = K_v i \tag{1}$$

where K_v is a constant representing the spool position against the input current. The direction and flow rate of the hydraulic pressure are determined according to the direction of the spool position x_v and the moving distance. When the spool moves, the hydraulic flow q_A into the hydraulic cylinder chamber A and the hydraulic flow out of the hydraulic cylinder chamber B are generated. The generated oil pressure moves the piston inside the cylinder, and the nozzle angle of the water-jet is changed by the movement of the piston.

Assume that the valve orifices are matched and symmetrical, the orifice areas are linear with the valve stroke, and the compressibility flows are zero. The control flow equation of the hydraulic valve for the load flow rate can be written as

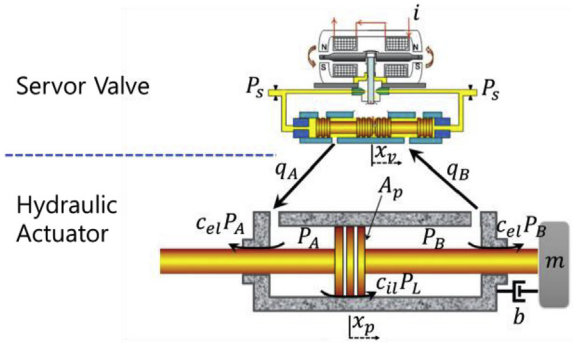

Fig. 1. Configuration of the hydraulic servo system.

$$Q_L = C_d w x_v \sqrt{\frac{P_s - P_L \mathrm{sgn}(x_v)}{\rho}} \tag{2}$$

where $Q_L(m^3/s)$ is the load flow rate, C_d is the discharge coefficient, w (m^2/s) is the area gradient of the servo valve spool, P_s (bar) is the supply pressure of the pump, P_L (bar) is the load pressure of the piston, and $\rho(kg/m^3)$ is the liquid density in the chamber.

Applying the law of continuity to each chamber, the load flow continuity equation is given as

$$A_p \dot{x}_p + C_{tl} P_L + \frac{V_t}{4\beta_e} \dot{P}_L = Q_L \tag{3}$$

where A_p is the pressure area of the piston, x_p represents the position of the piston, $0 < p < 1$ is the pressure area of the piston, $C_{tl} = C_{il} + C_{el}/2(m^5/Ns)$ is the total leakage coefficient, C_{il} is the internal leakage coefficient, C_{el} is the external leakage coefficient, $V_t(m^3)$ is the total actuator volume, and $\beta_e(N/m^2)$ is the effective bulk modulus of the system.

Using Eq. (2) and Eq. (3), the following fluid dynamic equation of the actuator is derived:

$$\dot{P}_L = -\frac{4\beta_e A_p}{V_t}\dot{x}_p - \frac{4\beta_e C_{tl}}{V_t} P_L + \frac{4\beta_e C_d w k_v i}{V_t}\sqrt{\frac{P_s - P_L \tanh(x_v)}{\rho}} \tag{4}$$

where $sign(x_v)$ is replaced by $\tanh(x_v)$ (Jerouane and Lamnabhi-Lagarrigue, 2001; Alleyne and Liu, 2000; Kaddissi et al., 2007).

In Fig. 1, the dynamic equation of the hydraulic actuator can be defined as follows (Yao et al., 2000):

$$m\ddot{x}_p + b\dot{x}_p + kx_p + F_d = A_p P_L \tag{5}$$

In Eq. (5), m is the mass of the nozzle connected to the hydraulic actuator, b is the damping coefficient of the hydraulic actuator, k is the spring coefficient of the hydraulic actuator, and F_d is the disturbance. To combine Eqs. (4) and (5), Eq. (6) is differentiated on both sides.

$$m\dddot{x}_p + b\ddot{x}_p + k\dot{x}_p + F_d = A_p \dot{P}_L. \tag{6}$$

Finally, the hydraulic servo system can be modeled as a third-order system whose state variables are designed as follows:

$$\begin{aligned} x_1 &= x_p \\ x_2 &= \dot{x}_p \\ x_3 &= \ddot{x}_p \\ u &= i \end{aligned} \tag{7}$$

Thus, the state equations are written as follows (Zeng and Sepehri, 2008):

$$\begin{aligned} \dot{x}_1 &= x_2 \\ \dot{x}_2 &= x_3 \\ \dot{x}_3 &= -f(x) + k_u u - d(t) \end{aligned} \tag{8}$$

where $f(x) = a_1 x_1 + a_2 x_2 + a_3 x_3$, $a_1 = \frac{4\beta_e C_{tl}}{mV_t}$, $a_2 = \frac{k}{m} + \frac{4\beta_e A_p^2}{mV_t} + \frac{4\beta_e C_{tl} b}{mV_t}$, $a_3 = \frac{b}{m} + \frac{4\beta_e C_{tl}}{V_t}$, $k_u = \frac{4\beta_e C_d A_p w k_v}{mV_t}\sqrt{\frac{P_s - P_L \tanh(x_v)}{\rho}}$ and $d(t) = -\left(\frac{4\beta_e C_{tl}}{mV_t}F_d + \frac{1}{m}\dot{F}_d\right)$.

Assumption. 1. The disturbance $d(t)$ is bounded and there exists a positive unknown constant δ_d satisfying $|d_i(t)| \le \delta_d$.

3. Proposed robust sliding mode control algorithm

The proposed algorithm is illustrated in Fig. 2 as a block diagram. The desired input, x_d, is generated by the off-line simulator for the SMC. After the control signal, u, is applied to the hydraulic actuator, the displacement, x, is measured using an encoder of the hydraulic actuator. Using the output x, the state observer estimates the state variables $\hat{x}_1$, $\hat{x}_2$, $\hat{x}_3$, $\hat{\hat{x}}_1$, $\hat{\hat{x}}_2$ and $\hat{\hat{x}}_3$ which are feed back to the SMC. Thus, the estimated state variables $\hat{x}_3$ and $\hat{\hat{x}}_3$ are sent to the disturbance observer to estimate the disturbance, $\hat{d}(t)$, which is finally fed back to the SMC.

3.1. Design of sliding mode control

The sliding surface is defined as

$$s = e_3 + c_2 e_2 + c_1 e_1 \tag{9}$$

where $c_i,\ i = 1, 2$ are positive constants and

$$\begin{aligned} e_1 &= x_{1d} - x_1 \\ e_2 &= \dot{e}_1 = x_{2d} - x_2 \\ e_3 &= \dot{e}_2 = x_{3d} - x_3 \quad . \end{aligned} \tag{10}$$

The time derivative of Eq. (9) can be expressed as

$$\begin{aligned} \dot{s} &= \dot{e}_3 + c_2 \dot{e}_2 + c_1 \dot{e}_1 \\ &= \dot{x}_{3d} + f(x) - k_u u + d(t) + c_2 e_3 + c_1 e_2 \quad . \end{aligned} \tag{11}$$

We define the Lyapunov function as follows:

$$V_1 = \frac{1}{2} s^2 \tag{12}$$

The time derivative of Eq. (12) becomes

$$\begin{aligned} \dot{V}_1 &= s\dot{s} \\ &= s[\dot{x}_{3d} + f(x) - k_u u + d(t) + c_2 e_3 + c_1 e_2] \end{aligned} \tag{13}$$

where $\hat{d}(t)$ is an estimation of $d(t)$ and $\tilde{d}(t) = d(t) - \hat{d}(t)$. We select the following control scheme:

$$u = \frac{1}{k_u}(u_{eq} + u_r) \tag{14}$$

where $u_{eq} = c_3 s + \dot{x}_{3d} + c_2 e_3 + c_1 e_2 + f(x) + \hat{d}(t)$, $u_r = \beta sign(s)$, c_3 and β are positive constants.

Substituting Eq. (14) into Eq. (13), we have

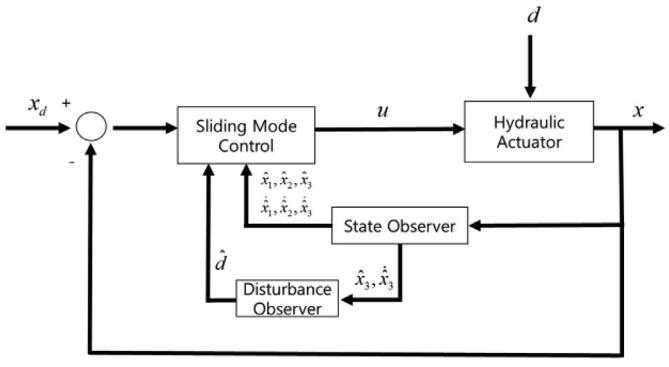

Fig. 2. Block diagram of the proposed algorithm.

$$\begin{aligned} \dot{V}_1 &= s\Big[\dot{x}_{3d} + f(x) - c_3 s - \dot{x}_{3d} - c_2 e_3 - c_1 e_2 - f(x) - \hat{d}(t) \\ &\qquad -\beta sign(s) + d(t) + c_2 e_3 + c_1 e_2\Big] \\ &= s\Big[-c_3 s - \tilde{d}(t) + d(t) - \beta sign(s)\Big] \\ &= -c_3 s^2 + s\tilde{d}(t) - \beta|s| \\ &\le s\tilde{d}(t) - \beta|s| \qquad \left(\because -cs^2 \le 0\right) \\ &\le |s|\tilde{d}(t) - \beta|s| \quad . \end{aligned} \tag{15}$$

If we select the control gain β as $\eta = \beta - \left|\tilde{d}\right| \ge 0$, we have

$$\dot{V}_1 \le -\eta|s| \le 0 \tag{16}$$

Therefore, the stability of the closed-loop system is satisfied.

However, in (14), the estimated disturbance $\hat{d}(t)$ cannot be known *a priori*, it needs to be estimated by the disturbance observer given in the next section.

3.2. Design of the state observer

The velocity x_2 and acceleration in Eq. (8) are not measurable directly. The velocity and acceleration information are obtained via differentiation of the position values measured by linear or rotary encoder scales and by differentiation of the velocity. These differentiations lead to a noisy velocity signal and require the low-pass filter to suppress the high-frequency noise. Thus, the velocity and acceleration signal qualities degrade and exhibit worse control performance. Therefore, the super-twisting state observer used in this study can assure better finite-time estimation error convergence than the conventional high-gain state observer. By using assumptions of the boundedness of $f(x)$ and $d(t)$, the super-twisting observer, which extends to the third order.

In this study, the third sliding mode state observer applied to the proposed algorithm is defined as follow:

$$\begin{aligned} \hat{\hat{x}}_1(t) &= \hat{x}_2(t) + z_1 \\ \hat{\hat{x}}_2(t) &= \hat{x}_3(t) + z_2 \\ \hat{\hat{x}}_3(t) &= h(t, \hat{x}_1, \hat{x}_2, \hat{x}_3, u) + z_3 \quad . \end{aligned} \tag{17}$$

In Eq. (17), $\hat{x}_1$, $\hat{x}_2$, $\hat{x}_3$ are the predicted state values by the state observer and $h(t, \hat{x}_1, \hat{x}_2, \hat{x}_3, u)$ is the predictive value defined as the right side of Eq. (8). Thus, z_1, z_2, z_3 are defined as correction variables as follow: (Davila et al., 2005).

$$\begin{aligned} z_1 &= \mu_1 |x_1 - \hat{x}_1|^{1/2} sign(x_1 - \hat{x}_1) \\ z_2 &= \mu_2 |x_1 - \hat{x}_1|^{1/2} sign(x_1 - \hat{x}_1) \\ z_3 &= \mu_3 sign(x_1 - \hat{x}_1) \end{aligned} \tag{18}$$

where z_1, z_2, z_3 are positive diagonal metrics.

From Eq. (17) and Eq. (18), we have the following state observer equation:

$$\begin{aligned} \hat{\hat{x}}_1(t) &= \hat{x}_2(t) + \mu_1 |x_1 - \hat{x}_1|^{1/2} sign(x_1 - \hat{x}_1) \\ \hat{\hat{x}}_2(t) &= \hat{x}_3(t) + \mu_2 |x_1 - \hat{x}_1|^{1/2} sign(x_1 - \hat{x}_1) \\ \hat{\hat{x}}_3(t) &= h(t, \hat{x}_1, \hat{x}_2, \hat{x}_3, u) + \mu_3 sign(x_1 - \hat{x}_1) \end{aligned} \tag{19}$$

where μ_i represents positive diagonal matrices. From Eq. (8) and Eq. (19), we have the following error state equations:

$$\begin{aligned} \tilde{x}_1 &= \tilde{x}_2 - \mu_1 |\tilde{x}_1|^{1/2} sign(\tilde{x}_1), \\ \tilde{x}_2 &= \tilde{x}_3 - \mu_2 |\tilde{x}_1|^{1/2} sign(\tilde{x}_1), \\ \tilde{x}_3(t) &= h(t, \tilde{x}_1, \tilde{x}_2, \tilde{x}_3) - \mu_3 sign(\tilde{x}_1) \end{aligned} \tag{20}$$

where $\tilde{x}_i = x_i - \hat{x}_i,\ i = 1,2,3$.

The boundedness of the system states ensures the existence of a constant C_h such that the inequality

$$|h(t,\hat{x}_1,\hat{x}_2,\hat{x}_3)| < C_h \tag{21}$$

holds for any possible t, $\hat{x}_1$, $\hat{x}_2, \hat{x}_3$, and $|\hat{x}_3| \le 2\sup|x_3|$ (Davila et al., 2005).

If the parameters μ_1, μ_2, and μ_3 in Eq. (19) are selected as the following conditions:

$$\begin{aligned} &\mu_3 > C_h \\ &\mu_2 > \sqrt{\frac{2}{\mu_3 - C_h}}\,\frac{(\mu_3 + C_h)(1+p)}{(1-p)} \\ &\mu_1 > \sqrt{\frac{2}{\mu_3 - C_h}}\,\frac{(\mu_3 + C_h)(1+p)}{(1-p)} \end{aligned} \tag{22}$$

where p is a constant satisfying $0 < p < 1$, then the variables of the observer in Eq. (21) converge to the states variables in Eq. (20) in finite time (Davila et al., 2005).

Using the state variable estimated using the super-twisting state observer in Eq. (20), the sliding mode surface can be defined as follows:

$$\hat{s} = \hat{e}_3 + c_2\hat{e}_2 + c_1\hat{e}_1 \tag{23}$$

where $c_i,\ i = 1,2$ are positive constants, $\hat{e}_1 = x_{1d} - \hat{x}_1$, $\hat{e}_2 = x_{2d} - \hat{x}_2$ and $\hat{e}_3 = x_{3d} - \hat{x}_3$.

The time derivative of Eq. (23) can be expressed as

$$\begin{aligned} \dot{\hat{s}} &= \dot{\hat{e}}_3 + c_2\dot{\hat{e}}_2 + c_1\dot{\hat{e}}_1 \\ &= \dot{x}_{3d} - f(\hat{x}) + k_u u - \hat{d}(t) + z_3 + c_2\hat{e}_3 + c_1\hat{e}_2 \quad . \end{aligned} \tag{24}$$

We define the Lyapunov function as follows:

$$V_2 = \frac{1}{2}\hat{s}^2 \tag{25}$$

The time derivative of Eq. (25) becomes

$$\begin{aligned} \dot{V}_2 &= \hat{s}\dot{\hat{s}} \\ &= \hat{s}[\dot{x}_{3d} + f(\hat{x}) - k_u u + d(t) + c_2\hat{e}_3 + c_1\hat{e}_2]. \end{aligned} \tag{26}$$

Therefore, the control input can be expressed as follows:

$$u = \frac{1}{k_u}(u_{eq} + u_r) \tag{27}$$

where $u_{eq} = c_3\hat{s} + \dot{x}_{3d} + c_2\hat{e}_3 + c_1\hat{e}_2 + f(\hat{x}) + \hat{d}(t) + z_3$ and $u_r = \beta sign(s)$.

Substituting Eq. (27) into Eq. (26), we have

$$\begin{aligned} \dot{V}_2 &\le -c_3\hat{s}^2 + \tilde{d}\hat{s} - \beta|\hat{s}| \\ &\le \left|\tilde{d}\right||\hat{s}| - \beta|\hat{s}| \\ &= -|\hat{s}|\left(\beta - \left|\tilde{d}\right|\right) \quad . \end{aligned} \tag{28}$$

If we select the control gain β as $\eta = \beta - \left|\tilde{d}\right| \ge 0$, we have

$$\dot{V}_2 \le -\eta|\hat{s}| \le 0 \tag{29}$$

3.3. Design of the disturbance observer

The USV is sensitive to changes in the direction of the ship when it is traveling at high speed and when the small nozzle angle changes. Such a sensitive steering change of the USV makes steady running difficult and consumes significant fuel, and hence, precise steering control is required. Water-jet nozzles are exposed to various disturbances such as algae, waves, and water streams from nozzles during ship operation. These various disturbances make precise steering control of the water-jet nozzle difficult. Therefore, robust control is required for the disturbances affecting the nozzle control of the water-jet. In the control algorithm proposed in this study, a disturbance observer is added for controlling the disturbances affecting the robust water-jet nozzle control. The disturbance observer used in this study is (The global exponential stability of the proposed Disturbance Observer (DO) is guaranteed by selecting design parameters depending on the maximum velocity and physical parameters.) A basic idea in the design of observers/estimators is to modify the estimation using the difference between the estimated and actual outputs.

Assumption 2. In this study, it is assumed that the disturbance $d(t)$ varies slowly comparing with the observer dynamics. Then, it follows that $\dot{d}(t) = 0$.

The third state equation in Eq. (8) can be expressed as follows:

$$d(t) = -f(x) + gu - \dot{x}_3 \tag{30}$$

The nonlinear disturbance observer is designed as follows (Chen et al., 2000):

$$\begin{aligned} &\hat{d}(t) = \psi(t) + \phi(x) \\ &\dot{\psi}(t) = -l\psi(t) - l[\phi(x) - f(x) + gu] \end{aligned} \tag{31}$$

where $\phi(x)$ is a nonlinear function to be designed. $l\,(x_3) = \partial\phi/\partial x_3$ is chosen such that $l(x_3) = \partial\phi/\partial x_3 > l > 0$. From the estimation error $\tilde{d}(t) = d(t) - \hat{d}(t)$, it follows that

$$\begin{aligned} \dot{\tilde{d}}(t) &= \dot{d}(t) - \dot{\hat{d}}(t) \\ &= -\dot{\hat{d}}(t) = -\dot{\psi}(t) - \frac{\partial\phi}{\partial x_3}\dot{x}_3 \\ &= l\psi(t) + l[\phi(x) - f(x) + gu] - l\dot{x}_3 \\ &= -l[\psi(t) + \phi(x)] + ld(t) \\ &= -l\hat{d}(t) + ld(t) \end{aligned} \tag{32}$$

Therefore, based on (32), thee observer error is governed by

$$\dot{\tilde{d}}(t) + l\tilde{d}(t) = 0 \tag{33}$$

(33) means that $\tilde{d}(t)$ is globally exponentially convergent with a decaying rate of at least e^{-lt} as $t \to \infty$. Thus, the system Eq. (32) is exponentially stable for all x and the disturbance estimate $\hat{d}(t)$ approaches $d(t)$ exponentially as time goes to infinity. In this study, $\phi(x)$ is selected as $\phi(x) = k_d x_3$, where $k_d > 0$ is a constant.

Using this Assumption, the error between the predicted disturbance and the actual disturbance is obtained using Eq. (32).

The error in the disturbance is reduced by using Eq. (33), and thereafter, the reduced disturbance error is applied to the state observer. Thus, the error in the disturbance approaches zero by repetitive calculation of the coupled state observer and the disturbance observer. As the actual physical disturbance changes more slowly than the computation speed of the present system, the disturbance estimation method based on the iterative calculation proposed in this study does not cause a problem in system control.

4. Experimental environment

Fig. 3 illustrates the configuration of the USV steering control system. The power required for operating the hydraulic pump is generated by the engine. The power generated by the engine is transmitted to the hydraulic pump through the shaft to drive the hydraulic pump. The pressure of the hydraulic system is generated by the operation of the hydraulic pump. The personal computer produces the control command signal, which is sent to the interface DSP (DAQ tool). Subsequently, the interface DSP generates a signal to control the servo valve. The servo valve controls the operation oil entering the piston. The piston, which is a hydraulic actuator, controls the nozzle.

The piston position sensor attached to the hydraulic piston sends the position value to the interface DSP. The piston position value is subsequently sent to the personal computer.

Table 1 shows the actual system parameter values used in the modeling and control algorithms.

The test bed designed to test the proposed algorithm is illustrated in Fig. 4.

This test bed was installed in a scientific water tank.

Fig. 5 shows the configuration of the test bed for the test USV steering system. In Fig. 5, the front of the test bed shows the engine, fuel tank, and battery and the rear of the test bed shows the water-jet, hydraulic pump, and servo valve.

Fig. 6 shows the disturbance generation system. The water flow generator is installed to create disturbance. It is installed 50 cm from the nozzle of the water-jet, which creates the water flow of approximately 2 m/s. The water-jet is set to approximately 2,000 rmp.

5. Experimental results

Fig. 7 shows the experiment result obtained using the PID algorithm. In Fig. 7, the red line is the reference water-jet angle signal. The signal range is 0–75 mm, which matches the angle of the water-jet nozzle of approximately −25°–25°. The blue line is the output from the PID control. For the PID control, the P gain is 2, the I gain is 0.5, and the D gain is 0.1.

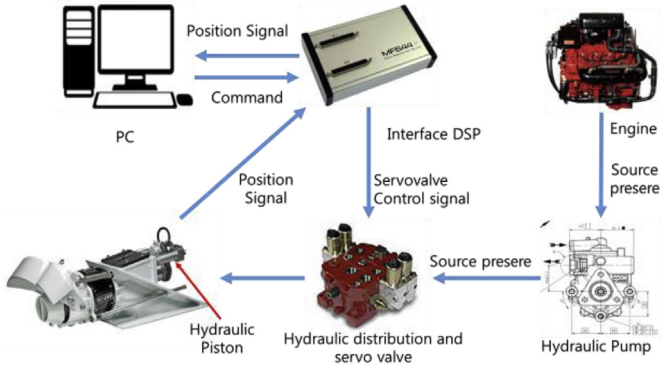

Fig. 3. Configuration of the control system.

Table 1
Control system parameters.

Symbol	Definition	Value
$0 < p < 1$	pressure area of the piston	7.07×10^{-4}
$Q_L(m^3/\text{min})$	load flow rate	6.70
C_d	discharge coefficient	0.61
$P_s(bar)$	supply pressure of the pump	100.01
$\rho(kg/m^3)$	liquid density in the chamber	9.01
$V_t(m^3)$	total actuator volume	5.30×10^{-5}
$m(kg)$	mass of nozzle	3.37

Fig. 4. Test bed of the USV steering system.

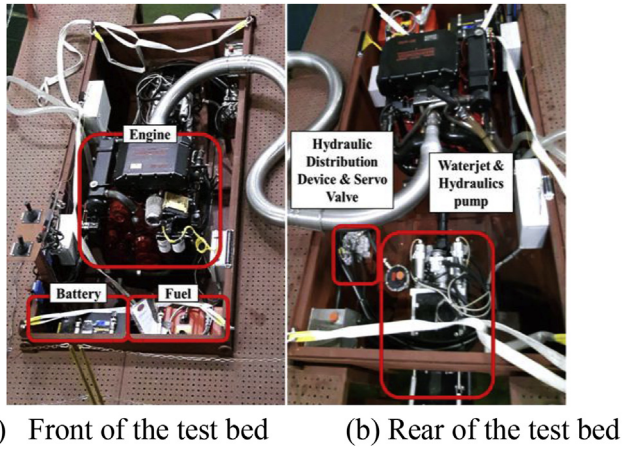

Fig. 5. Configuration of the test bed.

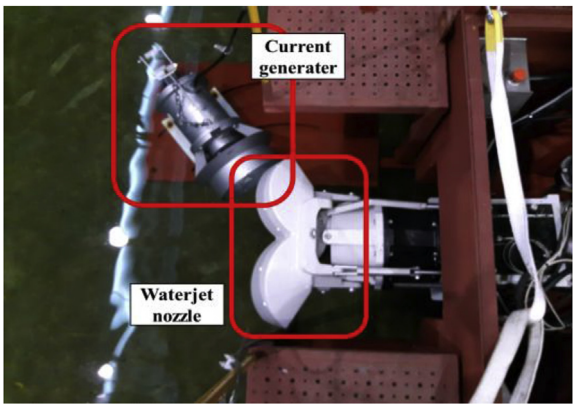

Fig. 6. Flow generator and water-jet.

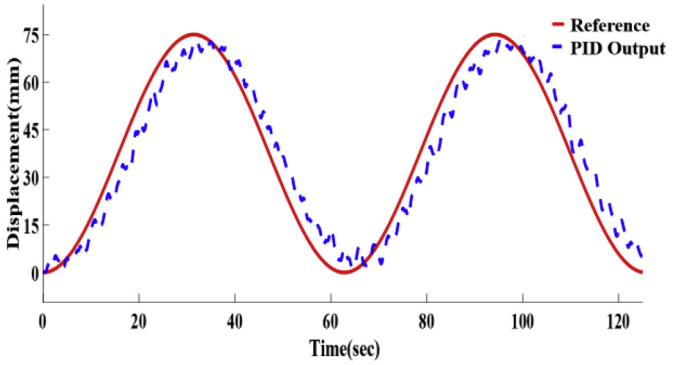

Fig. 7. Tracking using the PID algorithm.

Fig. 8 shows the output graph of SMC S/D-Ob output, which is the output of the SMC with the observer. It is better to apply the SMC with observer than to apply the PID algorithm. However, the error cannot be eliminated owing to the delay response characteristic of the hydraulic system. Fig. 9 shows the graph that compares the errors of the PID algorithm and the SMC with state observer. It can be observed that the proposed sliding mode algorithm with observer shows less error (maximum 9.5 mm) than the PID algorithm (maximum 14.5 mm).

The second experiment compares the control performance of the system when a step input occurs. Fig. 10 shows the result of comparing the PID controller with the output of the controller proposed in this study when a displacement input of 37.5 mm is given. In Fig. 10, SMC S/D-Ob output refers to the output of the sliding mode including the state observer and disturbance observer controlled in this study. The rising time of SMC S/D-Ob output is 1.15 s and the rising time of PID output is 1.32 s. Therefore, we can confirm that the rising time of the SMC S/D-Ob algorithm is faster. The SMC S/D-Ob output has a steady-state error of 0.32 mm, and the PID output has a steady-state error of 1.28 mm. In this study, the rising times were decided based on 100% criterion of the rising time that the output tracks the given reference command and the steady state errors were decided based on 2% tracking error criterion.

The third experiment is the result of comparing the output of the SMC including only the state observer and the output of the SMC including the state observer and disturbance observer, given the same input as the second experiment. In Fig. 11, SMC S/D-Ob represents the output of the SMC including the state observer and disturbance observer, and SMC S-Ob represents the output of the SMC including only the state observer.

In Fig. 11, the rising time of SMC S/D-Ob output is 1.15 s and the rising time of SMC S-Ob output is 1.25 s. Therefore, we can confirm that the rising time of the SMC S/D-Ob algorithm is faster. The SMC S/D-Ob output has a steady-state error of 0.32 mm, and the SMC S-Ob output has a steady-state error of 0.58 mm.

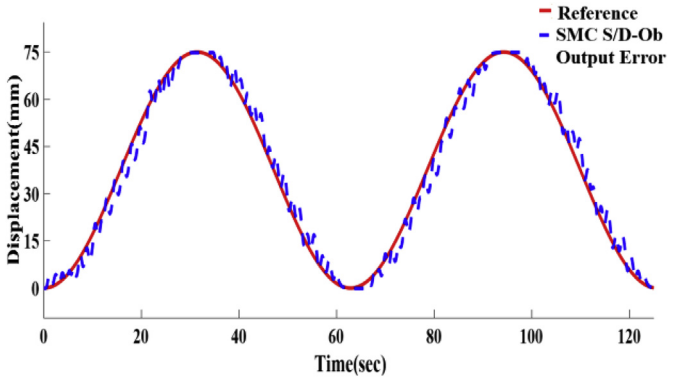

Fig. 8. Tracking using the proposed SMC.

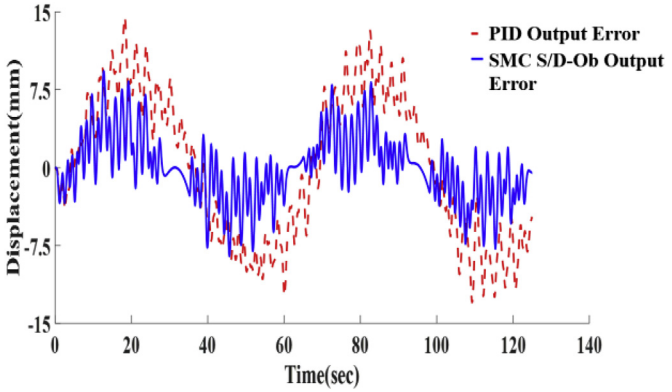

Fig. 9. Comparison of control errors of the PID and the proposed SMC algorithms.

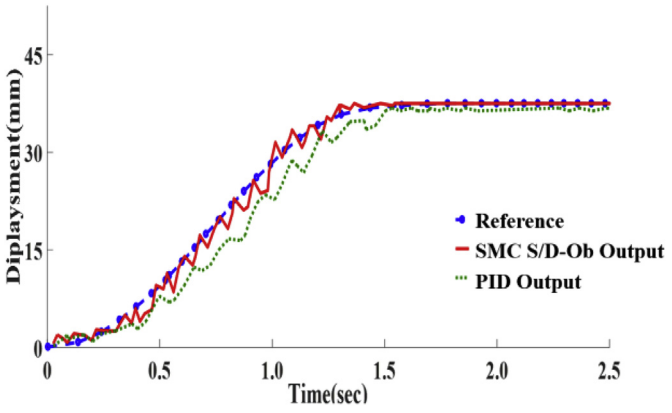

Fig. 10. Comparison between the PID and the proposed SMC.

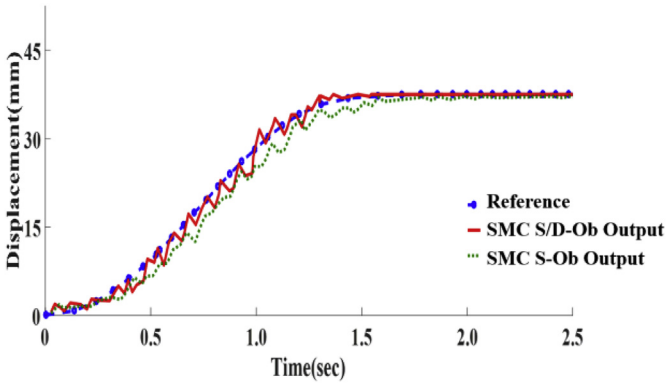

Fig. 11. Comparison between SMC with the state observer and the proposed SMC.

6. Conclusions

In this study, a robust SMC was designed for the position control of a hydraulic cylinder for a USV water-jet system and the efficiency of the controller was confirmed by comparing it with that of the conventional PID algorithm. The hydraulic system was modeled through mathematical analysis to design an SMC that manages the

nonlinear properties of the hydraulic system. As the hydraulic system is subjected to nonlinear dynamics and disturbances, the state and disturbance observers are added to the control feedback loop to improve the tracking performance. The response time of the hydraulic system can be further improved with better design of the SMC and the observers considering the specifications of the hydraulic cylinder.

References

Alleyne, A., Liu, R., Dec. 2000. A simplified approach to force control for electro-hydraulic systems. Contr. Eng. Pract. 8 (12), 1347–1356.

Bingham, Brian, et al., 2010. Robotic tools for deep water archaeology: surveying an ancient shipwreck with an autonomous underwater vehicle. J. Field Robot. 27 (6), 702–717.

Chen, T., Wu, Y., Oct. 1992. An optimal variable structure control with integral compensation for electrohydraulic position servo control systems. IEEE Trans. Ind. Electron. 39 (5), 460–463.

Chen, Wen-Hua, et al., 2000. A nonlinear disturbance observer for robotic manipulators. IEEE Trans. Ind. Electron. 47 (4), 932–938.

Davila, Jorge, Fridman, Leonid, Levant, Arie, 2005. Second-order sliding-mode observer for mechanical systems. IEEE Trans. Autom. Control 50 (11), 1785–1789.

GONG, Zhenghua, et al., 2017. Global sliding mode control approach for the steering system of the water-jet propulsion device. J. Shanghai Jiaot. Univ. 6, 008.

Huntsberger, Terry, Woodward, Gail, 2011. Intelligent autonomy for unmanned surface and underwater vehicles. In: OCEANS 2011. IEEE.

Iwan, Istanto, et al., 2017. Performance improvement of electro-hydraulic servo-valves by applying sliding mode control. In: KSFC Conference, pp. 63–69.

Jerouane, M., Lamnabhi-Lagarrigue, F., Dec. 2001. A new sliding mode controller for a hydraulic actuators. Proc. IEEE Conf. Dec. Control 1, 908–913.

Kaddissi, C., Kenne, J., Saad, M., Feb. 2007. Identification and real-time control of an electrohydraulic servo system based on nonlinear backstepping. IEEE ASME Trans. Mechatron. 12 (1), 12–22.

Merrit, H.E., 1967. Hydraulic Control System. Wiley and Sons, New York.

Son, Nam-Sun, Yoon, Hyeon-Kyu, 2009. Study on a waypoint tracking algorithm for unmanned surface vehicle (USV). J. Navig. Port Res. 33 (1), 35–41.

Utkin, Vadim, Guldner, Jürgen, Shi, Jingxin, 2009. Sliding Mode Control in Electro-Mechanical Systems. CRC press.

Wu, Gongxing, et al., 2009. The basic motion control strategy for the water-jet-propelled USV. In: Mechatronics and Automation, 2009. ICMA 2009. International Conference on. IEEE.

Yao, Bin, et al., 2000. Adaptive robust motion control of single-rod hydraulic actuators: theory and experiments. IEEE ASME Trans. Mechatron. 5 (1), 79–91.

Yoo, J.H., Ryu, J.K., 2016. Development of Steering System for Autonomous Unmanned Surface Vehicle, vol. 2016. KSPE, 49–49.

Yu-min, Xu, Yu-ru Su, Pang, Yong-jie, 2006. Expectation of the development in the technology on ocean space intelligent unmanned vehicles. Chin. J. Ship Res. 3, 001.

Zeng, H., Sepehri, N., Jan. 2008. Tracking control of hydraulic actuators using a LuGre friction model compensation. ASME J. Dyn. Syst. Meas. Control 130 (1), 014502-1–014502-7.